Measurement of the n-p elastic scattering angular distribution at $E_n = 10$ MeV

N. Boukharouba,[1,*] F. B. Bateman,[1,2,†] C. E. Brient,[1] A. D. Carlson,[3] S. M. Grimes,[1] R. C. Haight,[2] T. N. Massey,[1] and O. A. Wasson[3]

[1]*Institute of Nuclear and Particle Physics, Department of Physics and Astronomy, Ohio University, Athens, Ohio 45701*

[2]*Los Alamos National Laboratory, Los Alamos, New Mexico 87545*

[3]*National Institute of Standards and Technology, Gaithersburg, Maryland 20899*

(Received 18 October 2000; revised manuscript received 29 June 2001; published 18 December 2001)

The relative cross sections for scattering of neutrons by protons have been measured at $E_n = 10$ MeV for center-of-mass neutron scattering angles from 60° to 180°. Absolute differential cross section values were obtained by normalizing the angle-integrated relative angular distribution to the n-p total cross section. The angular distribution exhibits a backward enhancement consistent with an exchange component of the n-p interaction at this energy. The relative shape of the angular distribution is in good agreement with the prediction of the charge-dependent Bonn and Nijmegen potential models and with the Arndt phase-shift analysis. Better agreement is found with the evaluated nuclear data files (ENDF)/B-V than with the ENDF/B-VI evaluation.

DOI: 10.1103/PhysRevC.65.014004 PACS number(s): 13.75.Cs

I. INTRODUCTION

The nature of the nuclear force has been a central issue in nuclear physics especially since the discovery of the neutron by Chadwick in 1932 [1]. A description of this force has proved to be a daunting undertaking, and the first semiquantitative description [2] did not appear until 1957, a quarter century after Chadwick's discovery. However, a great deal of progress has been accomplished since then in understanding the nuclear force. This progress is reviewed in Refs. [3–6]. Most of what is known today about the nuclear force was obtained from measurements of the nucleon-nucleon (NN) interaction and the elastic angular distribution provides a test of the physics built in a given theoretical model. These measurements are used to refine theoretical models and phase-shift analyses and uncertainties in the results obtained from such analyses are affected by the limited data base. Over the last 70 years of investigations, a large body of precise p-p cross section data over a wide energy range was made available. That is not the case for the n-p cross section data, which are less accurate than the corresponding p-p data. This reduced accuracy was not a problem in the past, but, with the advent of high-precision potential models, phase-shift analyses, and sophisticated data evaluation methods in recent years [7–13], more accurate n-p cross section data are needed for a detailed test of their results. Moreover, the elastic n-p differential cross section involves both isoscalar ($T=0$) and isovector ($T=1$) components of the NN interaction, while the the p-p cross section involves only the isovector component.

Despite the importance of the n-p elastic scattering cross section, there is some disagreement concerning its behavior at neutron energies below 15 MeV. In the past, the n-p angular distribution was considered to be isotropic in the center-of-mass system, at or below 10-MeV neutron energy. However, theoretical model calculations [7,9,11,14–16], phase-shift analyses [17,18], and data evaluations [12,13] indicate the existence of a degree of anisotropy in the differential cross section, whose magnitude and shape are still open to discussion.

At the present time, data for the n-p differential cross section with 1–2 % overall uncertainty are available in the energy region above 20 MeV. Below 20 MeV, the best available data sets [19–25] are clustered around 14 MeV and generally characterized by large error bars. Even accounting for these large uncertainties, these data sets still differ significantly. These discrepancies influence evaluated nuclear data files (ENDF) where, for example, the two ENDF evaluations [12,13] show discrepancies of about 2% at 10 MeV. The predictions obtained from the Arndt phase shifts [17,18], the Nijmegen [7,9,14,16], and the full Bonn and charge-dependent Bonn (CD Bonn) [11,15] potentials are in excellent agreement at 10 MeV but no elastic scattering data are available to check these predictions or to aid in making a choice between the ENDF/B-V and ENDF/B-VI evaluations. A comparison of these predictions is shown in Fig. 1.

To remedy this unsatisfactory situation, improve our knowledge of this important cross section, and test the various predictions, a high-precision ($\approx 1\%$) measurement was needed. To this end, the present measurements were made of the shape of the hydrogen differential cross section at 10-MeV neutron energy. The absolute differential cross section is obtained from these data by normalizing the angle-integrated cross section to the total cross section. The only other open channel is radiative capture that has a very small cross section of 33 μb at this energy.

These measurements were made at the Institute of Nuclear and Particle Physics at Ohio University. The present work is a continuation of earlier measurements by this collaboration [26]. The relative differential cross section was measured at six angles simultaneously with telescopes containing solid-state ΔE-E detectors at each angle. To achieve a 1% overall uncertainty in the relative cross section and accurately use these data to normalize the results to the total

*Present address: Department of Physics, Chemistry & Physics Building, University of Kentucky, Lexington, KY 40506.

†Present address: National Institute of Standards and Technology, Gaithersburg, MD 20899.

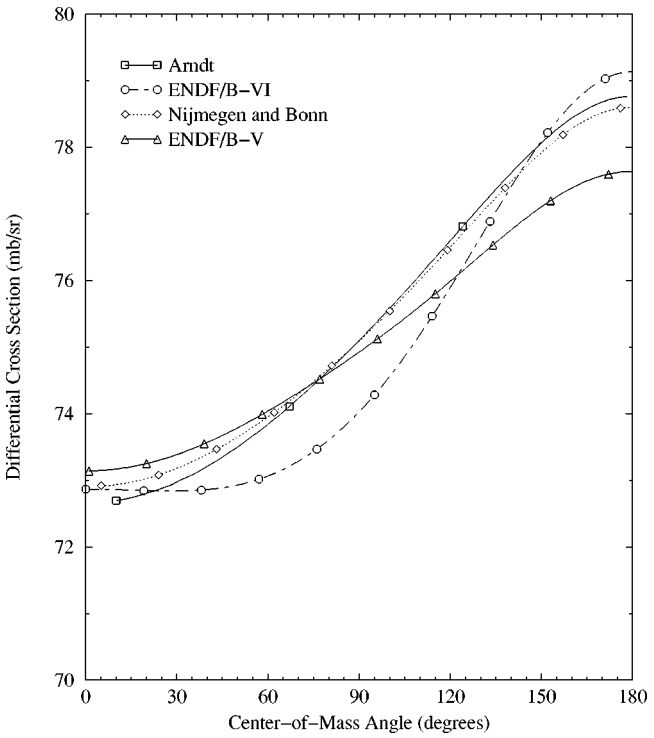

FIG. 1. Comparison of the predicted angular distribution for the n-p elastic scattering at 10 MeV (Refs. [12–15,17]).

cross section, the following criteria should be met: well-characterized monoenergetic neutron source, uniform hydrogenous target, independent consistency checks of the recoil-proton yields, an angular range as large as possible, precise angle and solid-angle determination, left-right asymmetry corrections, accurate background subtraction, relative neutron fluence monitoring in sample-in and sample-out runs, validated finite-size and multiple-scattering corrections, and a detector system that is optimized for each angle to match the recoil-proton energy.

These considerations were taken into account in the design of the experimental setup, data acquisition system, and analysis as described in detail in the following sections. All uncertainties quoted in this paper represent 1σ standard deviations.

II. EXPERIMENTAL DETAILS

A. Scattering chamber design

Two possibilities exist for measuring the n-p elastic scattering cross section depending on which of the scattered particles is detected. Most neutron elastic scattering cross sections were measured in the past by detecting the scattered neutrons. The precision of this method is highly dependent on an accurate determination of a neutron detection efficiency that is sensitive to energy. In n-p scattering, a significant fraction of the bombarding energy is carried away by the recoiling proton and the recoil energy varies rapidly with scattering angle. Contrary to neutron detection, the efficiency of detection of charged particles with solid-state detectors is very close to 100% and is nearly independent of energy, making detection of the recoil proton the preferred and more reliable method of measurement of this cross section.

Although detection of the recoil proton greatly simplifies the determination of the detector efficiency, the difficulty remains that the proton energy varies between the incident neutron energy and zero over the angular range of scattering. This has resulted in incomplete angular distributions, with most experiments around 14 MeV limited to the range of $0°$–$50°$ in laboratory proton angle.

To decrease backgrounds, it is customary to detect the proton in a counter telescope. The use of a pair of detectors, ΔE and E in coincidence, can significantly lower backgrounds both because dE/dx and energy are known, and because the telescope will not detect particles traveling at significant angles relative to the counter axis. Nearly all previous measurements utilized a single telescope that was sequentially moved to different angles spanning the angular range of the measurement. An obvious difficulty with this procedure is that the thicknesses of the ΔE and E detectors cannot be optimized for all angles. This problem is further compounded with the need to normalize the data to the incident neutron intensity for each angle.

Because of these limitations, it was decided to build a multitelescope scattering chamber specifically for this experiment. This allowed the detector thickness for both ΔE and E counters to be optimized for each angle. The goal was to obtain an angular distribution for recoil protons between $0°$ and $60°$ in the laboratory system, corresponding to a neutron scattering angle ranging from $60°$ to $180°$ in the center-of-mass system. This coverage is more complete than most of the previous 14 MeV data.

The neutron energy of 10 MeV was chosen for three reasons. First, there were no data in the literature at this energy. Second, the Ohio University Accelerator offers a strong source of neutrons at 10 MeV. And third, at an energy below 14 MeV, fewer partial waves are expected to contribute to the scattering leading to a more isotropic differential cross section and therefore reducing the problems associated with an incomplete angular distribution. At the same time, the flatter angular distribution makes more stringent demands on the precision of the measurement, since the expected variation of the center-of-mass differential cross section over the measured angular range is only 8%.

To provide a check of the alignment, detectors were located at $0°$ and on both sides of the beam at $\pm 12°$, $\pm 24°$, $\pm 36°$, $\pm 48°$, and $\pm 60°$. In addition to the advantage of allowing more flexibility in the choice of detector thickness, the multitelescope spectrometer increases the data acquisition rate. It averages out left-right asymmetries and provides a redundant set of independent measurements, which will decrease the overall uncertainty. Furthermore, the set of 11 independent ΔE-E telescopes removes problems associated with the necessity of a very accurate monitoring of the neutron beam intensity, which was required in a number of previous experiments for which data were taken one angle at a time.

B. Neutron Production and Collimation

The experimental layout is shown in Fig. 2. Quasimonoenergetic neutrons (full width at half maximum is 250

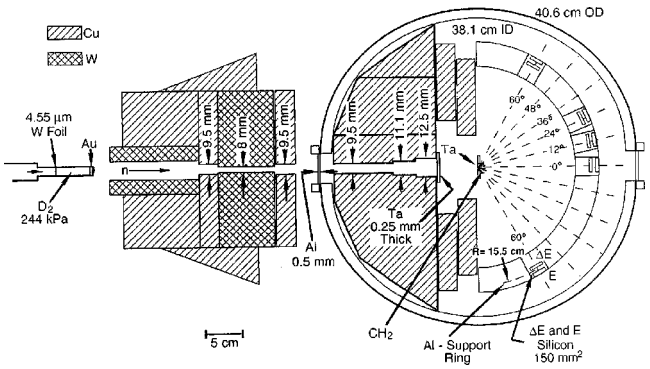

FIG. 2. Diagram of the apparatus used for the *n-p* elastic scattering measurements.

keV) were generated in a deuterium-filled gas cell using the ^{2}H$(d,n)^3$He reaction. The centroid energy was 10.04 MeV with an uncertainty of 20 keV. A continuous deuteron beam of 7.27 MeV was generated with the Ohio University Accelerator Laboratory's TM-11 tandem Van de Graaff accelerator and directed into a 4.42-cm long gas cell containing deuterium at a pressure of 276 kPa. This pressure was monitored and was not allowed to drift by more than 14 kPa. The gas cell entrance window was a 4.1-μm tungsten foil and a gold foil was used to stop the deuterons. Deuteron currents up to 8 μA were used. The neutron fluence was monitored with a stilbene detector, positioned at approximately 0° relative to the deuteron beam axis. Neutrons produced near 0° were collimated with appropriately shaped blocks of copper and tungsten, as shown in Fig. 2, such that the neutron flux over the CH_2 sample was uniform and its radial ''size'' was slightly greater than the CH_2 sample size of 10 mm. Neutron transport calculations were used in the design of the neutron shielding and collimation system. A radiograph of the neutron beam profile was taken and the beam was found to be centered at the center of the scattering chamber, and also to be visibly uniform over a diameter larger than that of the hydrogenous target. Collimation close to the sample (inside the scattering chamber) was needed to sharpen the edges of the neutron beam radial profile, and to significantly reduce the number of events in the silicon ΔE-E telescopes from stray neutron-induced charged-particle producing reactions. A sheet of tantalum covered the collimator to stop charged particles produced in the aluminum entrance window of the chamber and the neutron-collimation materials. Furthermore, deuteron breakup in the gas cell was investigated in a separate experimental run using a ^{3}He-filled gas cell. The neutron background from deuteron breakup on ^{3}He has been found [27] to be similar to that from deuteron breakup on deuterium. A negligible yield of pulses in the identification windows used for analyzing data was found for measurements with the ^{3}He cell.

C. Targets

In our previous work [26], the samples were attached to a 1-cm diameter tantalum collimator acting as a holder, with the sample on the side facing the neutron source. The material used to bond the sample to the tantalum was positioned behind the tantalum collimator and any charged particles produced in that material by neutron interactions would be stopped in the tantalum. Unfortunately, this geometry exhibited an increasing shadowing effect as a function of angle and was worst for the 60° telescopes. The reason for this is that at angles other than 0°, part of the sample was hidden from the detectors by the edges of the sample holder. Uncertainties in the calculation of the correction for this effect led to the use of a different target design. This alternate design used a circular film of polypropylene attached to a 0.5-mm thick tantalum plate, and facing the ΔE-E telescope. The tantalum plate, in this design, was merely used as a target support, and not a collimator; it helps keep the surface of the sample flat. A flat surface was especially important for the larger angles where a wavy film would induce a distortion in the detected recoil-proton spectrum and could possibly stop the recoiling proton in the case of the 60° angle.

The targets were made from CH_2 samples, obtained from commercial treated polypropylene, and bonded to the backing with a thin layer of ethyl cyanoacrylate. The charged particles produced from neutron interactions with the ethyl cyanoacrylate have less than 0.1% calculated effect on the cross sections obtained in the experiment. Because of the large recoil-proton energy difference between the small and the large angles, two thicknesses were used in the experiment, a thick sample (3.8×10^{-3}g/cm^2) for all angles except 60° to enhance the signal/background ratio, and a thin sample (1.4×10^{-3}g/cm^2) for all angles. This thin sample was required for the 60° angle where a minimum energy loss in the sample is desired. These films need only be analyzed for impurities, which were negligibly small, and not for absolute hydrogen content.

D. Alignment and angle determination

The scattering chamber, neutron collimator, and target ladder were carefully aligned with the beam line, using an optical telescope and a laser beam. Scattering angles for each individual telescope were then determined with the laser beam shining up the beam line through the telescope optical axis, and reflected from a mirror fitted onto a precision goniometer located at the center of the scattering chamber. The goniometer mirror was then rotated towards the detector in question until the reflected laser beam spot was at the center of the solid-angle-defining collimator situated in front of the ΔE detector. The laser beam was then turned off and the alignment viewed again through the optical telescope. The scattering angle was read from the goniometer with an estimated accuracy of $\pm0.1°$.

Relative solid-angle values for all telescopes were obtained by counting with a very thin and uniform ($\pm0.5\%$ variation over a 12.7 mm diameter) ^{239}Pu α particle source [28], placed at the sample position, and which had an area similar to that of the hydrogen scattering sample. Results of these measurements are shown in Fig. 3 for both of the independent data acquisition systems (see below) that were used in the measurement. There is excellent agreement between these two systems for the common detectors at $\pm12°$ and $\pm24°$, which were used to normalize the two indepen-

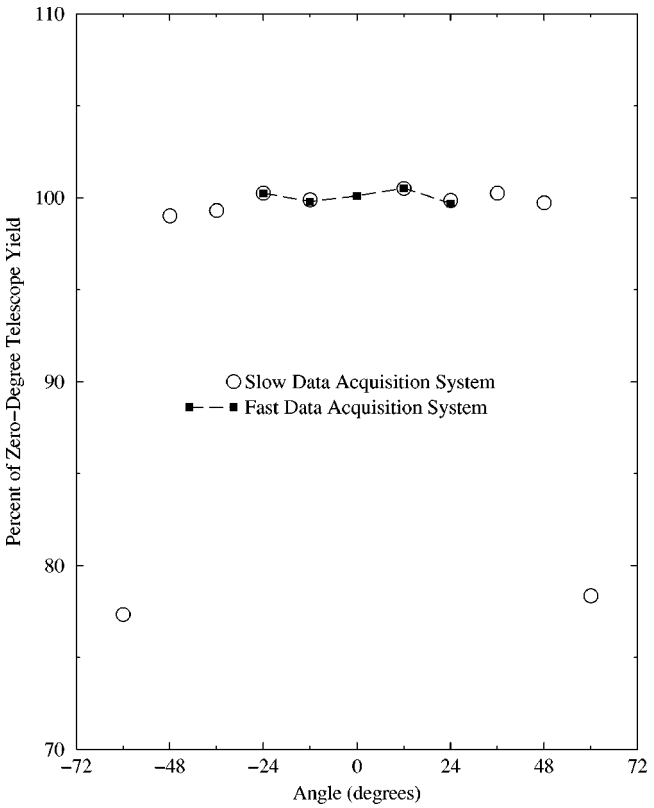

FIG. 3. Measurement of the α particle counting rates from a ^{239}Pu source for the determination of the relative solid angles.

dent data acquisition systems to each other.

The relative solid angles for the $\pm 60°$ telescopes were smaller in magnitude due to the narrower collimator used to reduce the kinematic energy spread of the recoil protons. This experiment does not require absolute measurements of the solid angles since only the shape of the angular distribution is measured.

E. The detector system

The 11 telescopes consisted of ΔE-E silicon surface barrier detectors positioned at $0°$, $\pm 12°$, $\pm 24°$, $\pm 36°$, $\pm 48°$, and $\pm 60°$ to the neutron beam axis. For each telescope, thicknesses for the ΔE and E detectors were chosen to obtain a maximum signal-to-noise ratio and minimum background from neutron-induced reactions in silicon. All detectors had an active area of 150 mm^2. This setup provides a good way to monitor any asymmetry in the neutron beam, hydrogenous target, or in the alignment.

It was determined, in a preliminary experimental run, that some modifications of the ΔE-E telescope geometry used in our previous work [26] were desirable. In that work, the solid-angle defining aperture consisted of a circular collimator located between the ΔE and the E detectors and flush against each of the detectors, which were held in place with Allen screws. Unfortunately, this simple design allowed small variations in the inclination of the collimator with respect to the target-detector axis when the ΔE detectors were removed to enable the relative solid-angle measurement, since all but the $60°$ ΔE detectors will stop 5-MeV α particles from the ^{239}Pu source. The variation in solid angle was estimated with a Monte Carlo program (discussed below). It was found that a slight change in the collimator inclination with respect to the telescope axis ($5°$ to $10°$) could yield a 2–10 % variation in the relative solid angle. To improve the reproducibility of the solid-angle measurement, tight-fitting aluminum sleeves were inserted flush against the front the ΔE detector to securely hold the E-ΔE collimator system. Another solid-angle-defining collimator was inserted in front of the ΔE detector in addition to the already existing larger collimator placed between the E and ΔE detectors. This layout, shown in Fig. 4, allowed the relative solid angle to be determined in a reliable way without the necessity of opening the scattering chamber and removing the ΔE detectors. For all angles other than $60°$, the front solid angle defining circular collimator had an inner radius of 0.47 cm, while the second larger collimator had an inner radius of 0.6 cm. The $60°$ collimator was in the shape of a rectangular aperture with rounded corners. The smaller side of the rectangle was positioned in the horizontal scattering plane in order to reduce the angular acceptance of the telescope. This configuration substantially decreased the kinematic energy spread, which is important at this angle and yielded better-defined recoil-proton peaks.

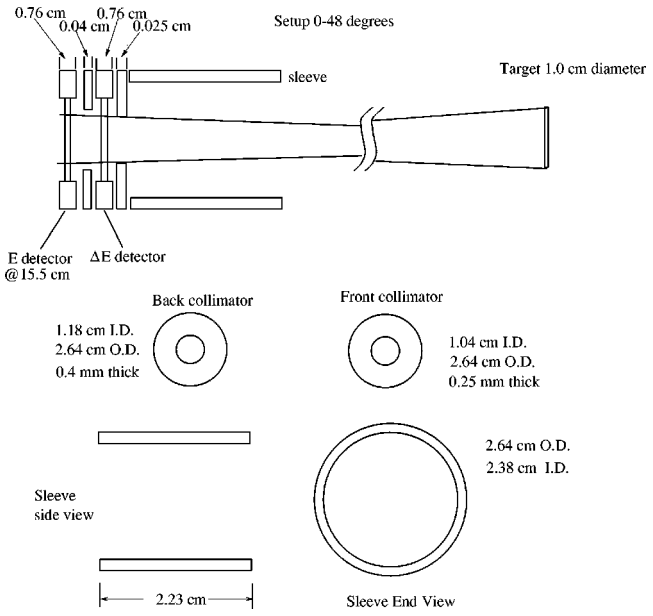

FIG. 4. Diagram of the detector assemblies and their collimator for the n-p elastic scattering measurements. For the detectors at $\pm 60°$, rectangular collimators were used. (See text.)

F. Electronics and data processing

The electronics consisted of two similar data acquisition systems. A ''slow'' system for all scattering angles with the exception of $0°$ and a ''fast'' system for $0°$, $\pm 12°$, and $\pm 24°$.

The purpose of these two systems was to reduce the dead time for the smaller angles where count rates were much higher than at the larger angles. Storing of data for the $\pm 12°$ and $\pm 24°$ detectors in both data acquisition systems permits

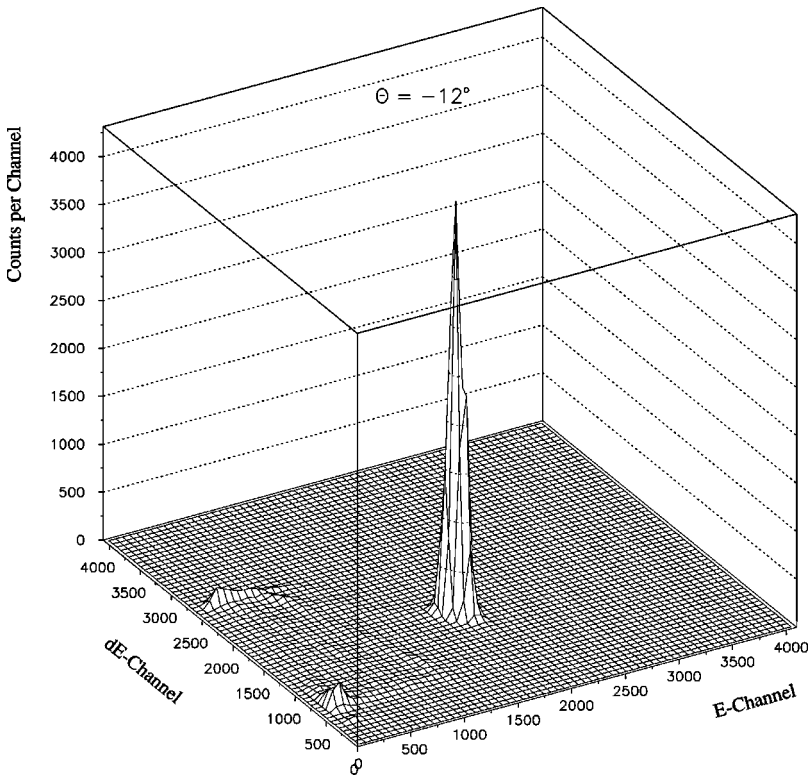

FIG. 5. Two-dimensional display of the pulse height distribution of the ΔE and E detectors obtained from a foreground run using the thick target and the fast data acquisition system.

the normalization of the two systems without concern for uncertainties in the calculation of dead time losses. Also, this redundancy allows consistency checks to be made. The main difference between the two systems was that timing signals were generated from a zero-crossover discriminator signal derived from the linear bipolar signal in the case of the ''slow'' system, whereas they were taken directly from the timing output of the preamplifier for the ''fast'' system. The two systems consisted of standard NIM [29] electronic modules. For each system, signals from the various detectors were multiplexed into a separate analog to-digital converter computer system. Each detector generated pulse height and timing information. Pulse height, timing, router, and stilbene neutron monitor signals were stored in an event buffer and subsequently written to disk for later off-line sorting and analysis.

A coincidence between E and ΔE signals was set in the hardware in order to minimize the background due to stray random events. Further background reduction was obtained by using the timing signals to generate relative timing information. A ''time-of-flight'' signal, henceforth ''TOF,'' was utilized to gate the event stream during off-line analysis. The purpose of this gate was to eliminate those events that met the ΔE-E coincidence requirement set in the hardware but fell outside the time window defined by the TOF gate. This proved most helpful in the case of the 0° and 12° scattering angles, where background levels were high and the rate of random ΔE-E coincidence occurrences was significant.

III. DATA ANALYSIS

A. Outline

The procedure used in the data analysis is outlined below. The digitized event stream was sorted by detector and protons were identified from the ΔE-E information. Legitimate events were those corresponding to protons recoiling with the appropriate energy. Further restriction was imposed by setting a TOF gate on all events that met the particle-type and energy requirements. The data set consists of several runs for both thin and thick target measurements, along with the corresponding background or blank run. A typical raw spectrum is shown in Fig. 5. Event data from the ''slow'' and the ''fast'' systems were treated as independent measurements and analyzed separately, then normalized to each other in the final stages of the analysis to obtain the complete relative angular distribution for a given target thickness. The normalization constant in this case was obtained from the average ratio of the proton yields for the telescopes at $\pm 12°$ and $\pm 24°$ for the ''slow'' and ''fast'' systems.

The general procedure used to obtain the recoil-proton yield was to form raw two-dimensional E vs ΔE and E vs TOF scatter plots and draw polygonal gates around the region of interest. The procedure was carried out on both the foreground and the background data. Neutron monitor rates determined the normalization coefficient used in the subtraction of the background from the foreground data. Relative solid-angle normalization was applied to the background-corrected recoil-proton yields using the relative solid-angle values obtained from the ^{239}Pu α source measurements. Typical results are shown in Figs. 6 and 7.

All corrections were then carried out individually for each detector and each target thickness. The results show good agreement between the beam-right and beam-left values. Relative angular distributions were obtained for each target thickness after averaging the beam-left and beam-right values. These distributions were then transformed to the center-of-mass system, using relativistic kinematics, fitted with a

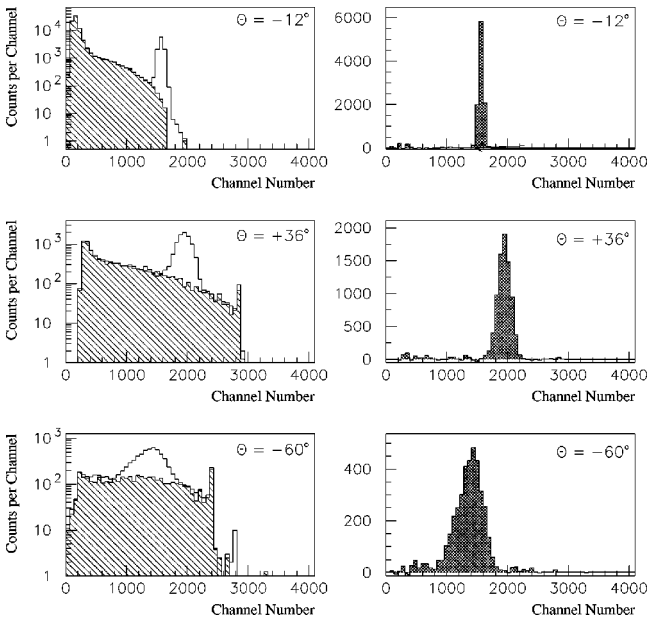

FIG. 6. Plot of the distribution of pulse heights from three detectors for events that satisfy the conditions set for legitimate recoil protons. The foreground as well as the normalized background data are shown on the left side of the figure, respectively.

Legendre polynomial, integrated, and finally normalized to the total elastic cross section.

B. Monte Carlo calculations

1. Description

A detailed investigation of the various parameters involved in this experiment was made necessary by the high-precision requirement. For this purpose, a Monte Carlo (MC) simulation program [30] was developed to assist in the design and analysis of this experiment, and to ascertain proton-loss mechanisms. The formalism used in the modeling of the atomic scattering of the ions is that of Ziegler and Biersack [31]. The program is flexible and can be used to investigate all aspects of the experiment, and can handle various species of light and heavy ions, as well as most types of amorphous multilayered scattering media. For the purpose of the present measurement, proton recoils are traced as they move through the sample, including scattering from carbon and hydrogen atoms within the target, and then, from the silicon atoms in the ΔE detectors. Statistics for the number of straight-line proton trajectories are stored, as well as those including atomic collisions. The percentage of proton losses due to multiple scattering, and the finite-geometry effects are estimated from the comparison of these two statistics. This program calculates many of the relevant parameters such as energy loss of the recoiling proton in the CH_2 sample and ΔE detectors, solid-angles subtended by the detectors at the target, effective scattering angles due to the finite target size, and straggling.

2. Monte Carlo validation

It is customary to test the predictions of a computer-simulation program in a validation procedure consisting of a direct statistical measurement. This was accomplished in a separate α particle counting experiment [30]. A brief description of the method used is given here. α particles from the thin ^{239}Pu source were counted with a single movable silicon solid-state detector, with the same geometry as that used in the n-p cross section measurement. An angular distribution was taken, with 0.3% statistics, for the angles of interest.

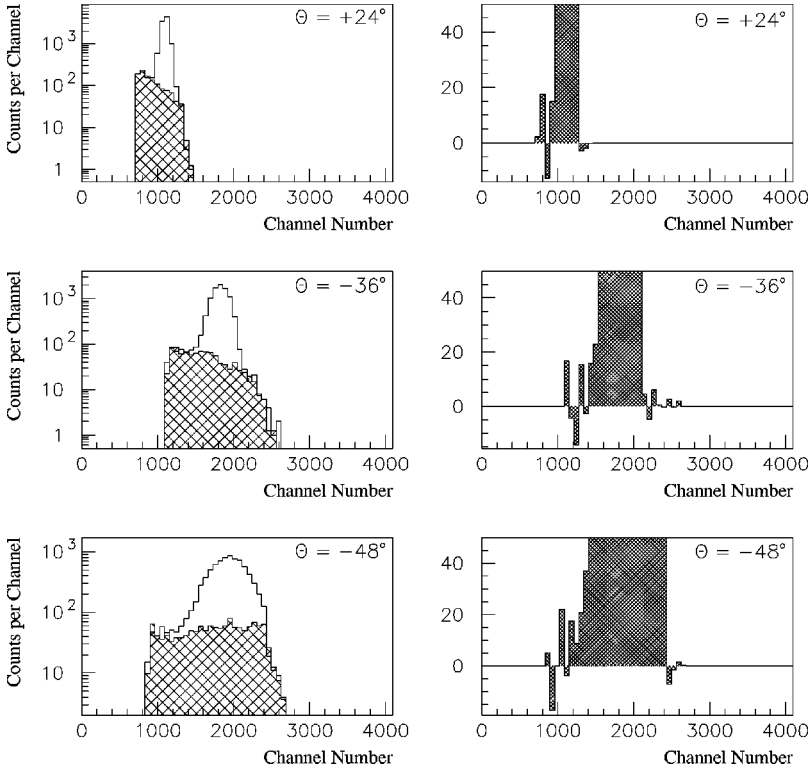

FIG. 7. Samples of gated and background-corrected histograms obtained using the thin target and the slow data acquisition system. The hatchs on the left plots illustrate the background overlay. The right column shows the background-corrected histograms magnified near the origin for a better view of the residuals.

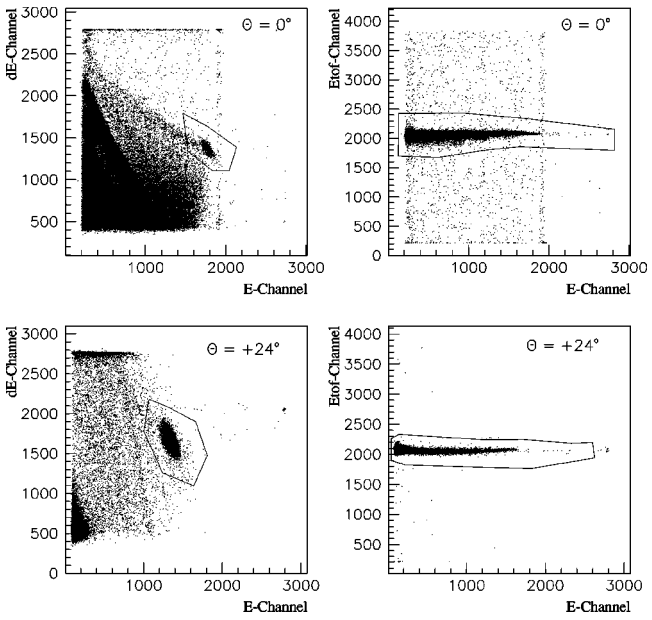

FIG. 8. Scatter plot of a set of typical two-dimensional gates (regions of interest) used to select the legitimate recoil protons.

Then thin mylar foils of different thicknesses were inserted in front of the α source, and the measurements were repeated. Mylar was used because it can easily be shaped into a thin flat foil, whereas polypropylene foils tend to sag and are difficult to maintain in a flat position. A comparison of the measurement without the mylar foils to one with mylar is a good estimate of the multiple scattering of the α particles within the mylar foils and its angular dependence. This configuration was modeled with the MC program whose predictions were then compared with the experimental results.

A very important first step was to test the assumption of isotropy of the ^{239}Pu α source, the validity of which is essential not only to the computer-simulation validation procedure, but also to the validity of the solid-angle determination method used in the n-p cross section measurement. A confirmation of this hypothesis was made by measuring the open-source angular distribution of α particles in the forward direction between $-60°$ and $+60°$. No measurable angular dependencies were found in this case, which indicates that the α source is truly isotropic within the angular range of interest, and that multiple scattering of the α particles within the radioactive medium and backing was not significant. This is consistent with the MC predictions for the ^{239}Pu source. Moreover, the calculated thickness deduced from the activity of the source is in excellent agreement ($\pm 0.5\%$) with the nominal value given by the manufacturer.

The MC predictions for the multiple scattering of α particles in mylar agree with the measurements to within 20% resulting in an error of less than 0.1%. These results, obtained for the case of α particles, indicate that the computer program is working properly, and should yield reliable predictions for protons.

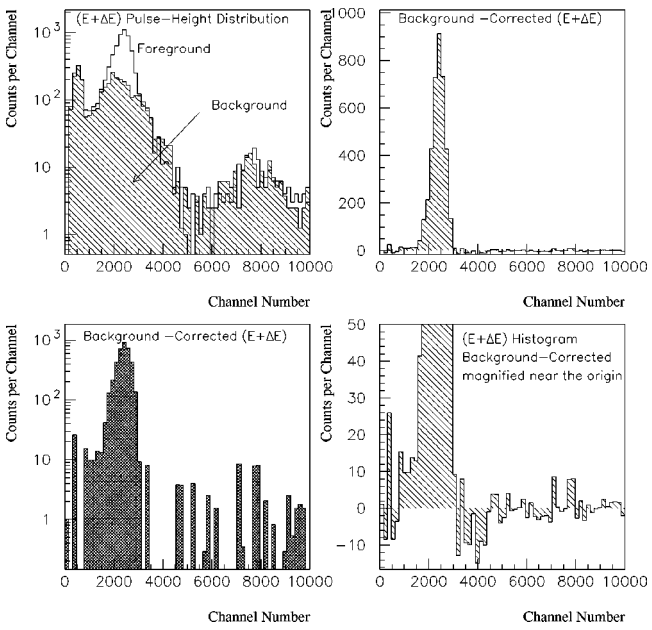

FIG. 9. Distribution of pulse heights for the sum $(E+\Delta E)$ for telescope $+60°$.

C. Corrections

Effects that have a bearing on the recoil-proton yields were explored in detail for each target and telescope. The uncertainty strongly affects the final accuracy of the measurement. Finite-size effects as well as multiple scattering in the hydrogen target and the ΔE detectors were calculated with the MC program, for both the thin and the thick target, and the results were used to correct the proton yields.

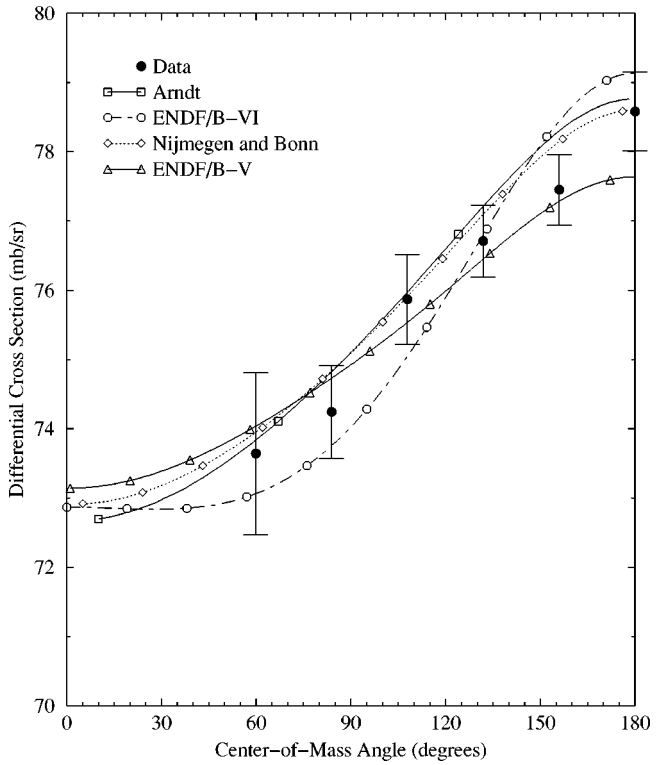

FIG. 10. Differential H(n,n) cross section at 10-MeV neutron energy compared to the predictions of Arndt, Nijmegen, Bonn, ENDF/B-V, and ENDF/B-VI.

TABLE I. Summary of experimental data. The values given in the table are obtained from a normalization of the measured angle-integrated cross section to the Breit-Hopkins [34] total elastic cross section value after radiative capture correction.

$\Theta_{c.m.}$	$\sigma(\Theta_{c.m.})$ (mb/sr)	$\Delta\sigma$ (mb/sr)
180.00	78.95	0.66
155.94	77.81	0.39
131.89	77.07	0.40
107.86	76.22	0.42
83.85	74.59	0.46
59.87	73.98	1.24

The ^{239}Pu α source used in the measurement of the relative solid angles and in testing the MC program, was checked and modeled to resolve a number of issues related to the multiple scattering of the α particles in the radioactive material and the size of that deposit. Multiple scattering within the source was completely negligible as discussed in the preceding section. Moreover, it was established that the difference in diameter between the ^{239}Pu source (1.27 cm) and the hydrogenous sample (1.0 cm) has no measurable effects on the solid-angle determination, largely because the source is extremely thin and uniform, and that the whole area of the deposit was seen by the ΔE-E telescope.

Calculations of proton counting losses from nuclear reactions in silicon at the proton energies under consideration showed that these were less than 0.1%, in agreement with Refs. [32,33].

Various E-ΔE and E-TOF gates of reasonable sizes and shapes (an example is shown in Fig. 8) were utilized to obtain the raw proton yields. Upon comparison, it appeared that these yields were, to a large extent, independent of any particular set of gates, except at 0° where a maximum of 0.9% difference in proton yield was obtained for different sets of E-ΔE gates. This was expected because of the larger level of background events for this telescope, which was directly in the path of the neutron beam. The E-TOF gate had little impact on the yields for angles larger than 12° where the spectra were very clean, but was very helpful in reducing the number of stray neutron events for the 0° telescope, and, to a lesser extent, for the 12° telescope. Its use also resulted in the reduction of uncertainties in proton yield due to the shape of the E-ΔE gate when both gates were applied simultaneously. The proton yields were in good agreement for all sets of gates used in the analysis.

Because of straggling, the 48° and 60° E detectors exhibited a residual tail in the recoil-proton peak after background subtraction. This tail was quite sizable, amounting to about 5% of the peak sum at 60°, and about 0.8% for 48°, both values resulting in an unacceptable overall uncertainty in the proton yield for these data points. These two angles are crucial to the accurate determination of the shape of the angular distribution. To alleviate this problem, the E and ΔE signals from the raw data were gain matched using the MC program, then summed to obtain the total recoil energy for each event. The analysis procedure outlined above was repeated, resulting in a dramatic reduction of the residual tail to about 0.6% of the total peak sum for the 60° right telescope, and only 0.2% for the 60° left telescope. The results are shown in Fig. 9 for the $+60°$ (beam-left) telescope.

All corrections were then performed individually for each detector and each target thickness. Relative angular distributions were obtained for each target thickness after averaging the beam-left and beam-right values. These distributions were then transformed to the center-of-mass system, using relativistic kinematics, fitted with a Legendre polynomial, integrated and finally normalized to the total elastic cross section of 943.2 mb as given by Hopkins and Breit [34]. It should be mentioned that ENDF/B-V [12] is the same as the Hopkins-Breit evaluation using the Yale phase-shift potentials.

IV. RESULTS AND DISCUSSION

The deduced angular distribution is shown in Fig. 10 and listed in Table I. The angular distribution is peaked in the backward direction, consistent with an exchange interaction, a virtual charged pion is exchanged between the proton and the neutron, thus exchanging their identities. There is no forward peak that would indicate a scattering from the tail of

TABLE II. List of estimated uncertainties. Other secondary sources of uncertainties (Monte Carlo corrections, foreground-background normalization, and solid-angle uncertainties) are not listed in the table, but are included in the value of the total estimated uncertainty, which relates to the shape of the angular distribution and does not include the total cross section normalization uncertainty.

$\Theta_{c.m.}$	Foreground statistical uncertainty (%)	Background statistical uncertainty (%)	Total statistical uncertainty (%)	Gate size uncertainty (%)	Total estimated uncertainty (%)
180.00	0.593	0.212	0.804	0.5	0.835
155.94	0.401	0.045	0.450	0.2	0.509
131.89	0.424	0.081	0.443	0.1	0.516
107.86	0.458	0.110	0.471	<0.1	0.554
83.85	0.520	0.160	0.544	<0.1	0.619
59.87	1.410	0.829	1.636	<0.1	1.665

TABLE III. Summary of χ^2 values obtained from the comparison of the data with the models. χ^2 is obtained from the experimental data points.

	χ^2
ENDF/B-V	2.17
ENDF/B-VI	2.54
Arndt SM94	0.47
Nijmegen-Bonn	0.48

the n-p potential in agreement with the results shown in Fig. 1. Figure 10 compares the data to some recent theoretical predictions and phase-shift analyses [9,11,18] and to the ENDF/B-V [12] and ENDF/B-VI [13] data evaluations using the total cross section value given by Hopkins-Breit [34] $\sigma_{\rm tot}=943.2$ mb to normalize the angular distribution. The estimated average uncertainty of the present measurement is better than 0.8%. Table II gives a list of of the most significant sources of errors. The best χ^2/datum is obtained when the three lowest-order Legendre polynomials are used to fit the data, with a small contribution from the third term.

The quantity

$$\chi^2=\frac{1}{N-1}\sum_{i=1}^{N}\left(\frac{\sigma_i^{experiment}-\sigma_i^{model}}{\Delta\sigma_i}\right)^2$$

is the comparison criterion used to determine which of the models and evaluations are in better agreement with the present data (see Table III). χ^2 corresponds to a comparison to the measured experimental data. The total n-p scattering cross sections and the ratios $\sigma(180°)/\sigma(60°)$ are also shown in Table IV which shows a disagreement in the correct value of the n-p total cross section of the order of $\approx 1\%$. In Ref. [5] in which the Nijmegen potential (and also the Paris potential [35]) was found to overestimate the n-p total cross in the energy range between 10 and 300 MeV, and a comparison to the experimental data using the Bonn B potential [3] yielded the lowest χ^2/datum. The potential models and the Arndt phase-shift analysis predict a larger total cross section than either ENDF/B-V or ENDF/B-VI data evaluations. For this reason the intermediate value of 943.2 mb was used to normalize the present data. It should be mentioned that in the comparisons listed in Table III, the angular distributions from the predictions (i.e., $\sigma^{\rm model}$) were renormalized using the value $\sigma_{\rm tot}=943.2$ mb, thus subtracting any effect due to the uncertainty in the total cross section value.

TABLE IV. Summary of n-p total cross sections values and $\sigma(180°)/\sigma(60°)$ ratios at 10 MeV from potential models, phase-shift analysis, and data evaluations obtained from Refs. [7,9,11–13,17]. The value listed for $\sigma_{\rm tot}$ for the present data is not a new measurement, but rather is the value to which the present relative cross sections were normalized.

	$\sigma_{\rm tot}$ (mb)	$\sigma(180°)/\sigma(60°)$
ENDF/B-V	943.2	1.049
ENDF/B-VI	938.2	1.083
Arndt-SM94	946.6	1.060
Nijmegen	946.5	1.062
CD Bonn	944.5	1.063
Present data	943.2	1.063

Good agreement with the present data was obtained for the CD Bonn [11] and Nijmegen [7] potentials, Arndt SM94 (phase-shift analysis) [17,18], and the ENDF/B-V [12] data evaluation, with a somewhat better agreement for the CD Bonn model and Arndt partial-wave analysis. The ENDF/B-VI [13] angular distribution does not appear to have the right angular dependence at this energy. Furthermore, its total cross section predictions are lower than most of the experimental data at this energy, for example, in Ref. [36] $\sigma_{\rm tot}=948$ mb. The ENDF/B-VI evaluation was strongly influenced by measurements at about 14-MeV neutron energy [21]. The publication of this work has been investigated and some serious problems were found with the analysis of that experiment. Pulse height distributions for the foreground and background measurements indicate that there were tails, events of lower pulse height, which have not been explained. It is difficult to evaluate errors associated with this. Also, the measurements were made at a time when it was difficult to make corrections for the effects resulting from proton scattering in the polyethylene target and the proportional counters used in the experiment. Unfortunately, the publication does not contain all the information necessary to calculate these corrections. Assuming that the drawing of the counter telescope (Fig. 3 of Ref. [21]) is drawn to scale, an estimate of the error introduced by not including these corrections was obtained with the Monte Carlo program used in the present experiment. This error is tentatively estimated at 2%. This error should be added in quadrature with the uncertainties shown for each data point in the publication. This will represent a lower limit since we have not assigned an error from the tails in the pulse height distribution. Additionally, errors were found in the center-of-mass angles used in their analyses, which we have corrected. In summary, uncertainties in the results of Ref. [21] seem to be larger than previously reported.

V. CONCLUSION

We have measured the shape of the H(n,n) scattering angular distribution between 60° and 180° in the center-of-mass system with an average uncertainty of better than 0.8%. The uncertainty in the neutron energy contributed less than 0.1% to this from variations of corrections with energy. The angular distribution is backward peaked, an indication of the dominance of the pion-exchange character of the n-p interaction at this energy. A least-squares Legendre polynomial fit to the measured differential cross section in the center-of-mass system requires S, P, and a small fraction of D waves be included for the best fit, and is expressed as

$$\sigma(\Theta_{\rm c.m.})=a_0+a_1P_1+a_2P_2,$$

where P_1 and P_2 are Legendre polynomials of order 1 and 2, respectively. The parameters of the least-square fit to the data are given (in mb/sr) as

$$a_0 = 75.06 \pm 0.43,$$

$$a_1 = -2.58 \pm 1.19,$$

$$a_2 = 0.60 \pm 0.95,$$

$$\chi^2/\text{d.o.f.} = 0.44.$$

The present data support the validity of the potentials of the Bonn [11,15] and Nijmegen [7,14] groups, the phase-shift analysis of Arndt [17,18], and the ENDF/B-V evaluation [12]. Among all these results, the charge-dependent nonlocal Bonn potential [11] gave the best overall agreement with the absolute cross section values derived from the present measurement (listed in Table I). The poorer agreement with ENDF/B-VI suggests there may be problems with the accuracy of the data at 14 MeV [21] that are not as accurate as claimed.

ACKNOWLEDGMENTS

The authors wish to acknowledge the assistance of D. E. Carter for his help with the electronics and data acquisition, D. Sturbois for accelerator maintenance, J. E. O'Donnell for help with accelerator operations and the preparation of the manuscript, and R. Wheeler and J. Oldendick for accelerator operations. We would also like to thank Professor Charlotte Elster for her help in the phase-shift calculations and David Gilliam for supplying the ^{239}Pu α source. This work was supported in part by the U.S. Department of Energy under Contract No. W-7405-ENG-36 and also in part by Department of Energy Grant No. DE-FG-02-88ER40387.

[1] J. Chadwick, Proc. R. Soc. London, Ser. A **136**, 692 (1932).
[2] J.L. Gammel and R.M. Thaler, Phys. Rev. **107**, 291 (1957); **107**, 1337 (1957).
[3] R. Machleidt, Adv. Nucl. Phys. **19**, 189 (1989).
[4] R. Machleidt and I. Slauss, J. Phys. G **27**, R69 (2001).
[5] R. Machleidt and G.Q. Li, Phys. Rep. **242**, 5 (1994).
[6] R. Machleidt, *Nuclear Structure 98*, edited by C. Baktash, AIP Conf. Proc. No. 481 (AIP, Woodbury, NY, 1999), p. 3.
[7] V.G.J. Stoks, R.A.M.M. Klomp, C.P.F. Terhegen, and J.J. de Swart, Phys. Rev. C **49**, 2950 (1994).
[8] R.B. Wiringa, V.G.J. Stoks, and R. Schiavilla, Phys. Rev. C **51**, 38 (1995).
[9] J.J. de Swart, R.A.M.M. Klomp, M.C.M. Rentmeester, and Th.A. Rijken, Few-Body Syst., Suppl. **8**, 438 (1995).
[10] R. Machleidt, F. Sammarruca, and Y. Song, Phys. Rev. C **53**, 1483 (1996).
[11] R. Machleidt, Phys. Rev. C **63**, 024001 (2001).
[12] L. Stewart, R.J. La Bauve, and P.G. Young, Summary Documentation for H in ENDF/B-V Summary Documentation, compiled by R. Kinsey, ENDF-201 (BNL-NCS-17541), BNL.
[13] G.M. Hale, D.C. Dodder, E.R. Siciliano, and W.B. Wilson, Summary Documentation for H in ENDF/B-VI Summary Documentation, compiled by P. F. Rose, ENDF-201 (BNL-NCS-17541), BNL.
[14] M.M. Nagels, T.A. Rijken, and J.J. de Swart, Phys. Rev. D **17**, 768 (1978).
[15] R. Machleidt, K. Holinde, and Ch. Elster, Phys. Rep. **149**, 1 (1987).
[16] URL: http://nn-online.sci.kun.nl
[17] R.A. Arndt, J.S. Hyslop, and L.D. Roper, Phys. Rev. D **35**, 128 (1987).
[18] R.A. Arndt, I.I. Strakovsky, and R.L. Workman, Phys. Rev. C **50**, 2731 (1994).
[19] J.C. Allred, A.H. Armstrong, and L. Rosen, Phys. Rev. **91**, 90 (1953).
[20] J.D. Seagrave, Phys. Rev. **97**, 757 (1954).
[21] T. Nakamura, J. Phys. Soc. Jpn. **15**, 1359 (1960).
[22] A. Suhami and R. Fox, Phys. Lett. **24**, 173 (1967).
[23] I. Basar, *Few-Body Problems, Light Nuclei and Interactions* (Gordon & Breach, New York, 1968), Vol. 2, p. 867.
[24] S. Shirato and K. Saitoh, J. Phys. Soc. Jpn. **36**, 331 (1974).
[25] W. Burkle and G. Mertens, Few-Body Syst. **22**, 11 (1997).
[26] R.C. Haight, F.B. Bateman, S.M. Grimes, C.E. Brient, T.N. Massey, O.A. Wasson, A.D. Carlson, and H. Zhou, Fusion Eng. Des. **37**, 49 (1997).
[27] S.M. Grimes, P. Grabmayr, R.W. Finlay, S.L. Graham, G. Randers-Pehrson, and J. Rapaport, Nucl. Instrum. Methods Phys. Res. **203**, 269 (1982).
[28] J. Van Audenhove, P. DeBievre, J. Pauweis, F. Petermans, M. Gallet, and A. Verbruggen, Nucl. Instrum. Methods **167**, 61 (1979).
[29] Nuclear Instrumentation Methods, U.S. Department of Energy Report DOE/ER-0457, 1964.
[30] N. Boukharouba, F.B. Bateman, C.E. Brient, A.D. Carlson, S.M. Grimes, R.C. Haight, T.N. Massey, and O.A. Wasson, Institute of Nuclear and Particle Physics Internal Report No. INPP00-01, 2000 (unpublished).
[31] J.F. Ziegler and J.P. Biersack, *The Transport of Ions in Matter* (IBM, Yorktown, New York, 1992).
[32] R.E. Pollock and G. Schrank, Phys. Rev. **140**, B575 (1965).
[33] J.J. Kraushaar, R.A. Ristenen, and R. Smythe, Phys. Lett. **25B**, 13 (1967).
[34] J.C. Hopkins and G. Breit, Nucl. Data Tables **9**, 137 (1971).
[35] M. Lacombe, B. Loiseau, J.M. Richard, R. Vinh Mau, J. Cote, P. Pires, and R. de Tourreil, Phys. Rev. C **21**, 861 (1980).
[36] R. Clement, Nucl. Phys. **A183**, 51 (1972).